Organic Sensor Array Distributed in Flexible and Curved Surface

Masatoshi Sakai[*,1], **Yugo Okada**[2], **Yuichi Sadamitsu**[3], **Yuta Hashimoto**[3], **Nozomi Onodera**[3], **Kazuhiro Kudo**[1]

[1] Department of Electrical and Electronic Engineering, Chiba University, Chiba city, Japan
[2] Center for Frontier Science, Chiba University, Chiba city, Japan
[3] Center for Innovative Research and Development Group Nippon Kayaku Co., Ltd., Tokyo, Japan

Key words: Organic semiconductor, Flexible electronics, Curved surface, Sensor, Artificial tactile sense, 3D printer

* Corresponding author: e-mail sakai@faculty.chiba-u.jp

Organic sensor array was fabricated on a curved plastic film substrate of which Gauss curvature was finite. In this work, we proposed soft robot finger as one of the test cases of curved surface device that has artificial tactile sense by detecting slight deformation induced by touching an object. We made curved surface sensor array by thermal molding of planer device array on thin plastic film. Observed electrical current in each sensor pixel reflected strain distribution and time response induced by external slight displacement applied.

1 Introduction Recently, flexible and stretchable electronics attract much interest in the field of electronic devices[1–17]. Although electronics on a curved surface have been investigated by sticking flexible or stretchable electronics onto the curved surface, the curved surface is geometrically different from the simple plane. So it is not easy to stick a planer flexible device on the curved surface perfectly. Stretchable device is also a candidate for the electronics on the curved surface, however, stretchable devices have a drawback that they cannot keep the shape without an object[18]. In this work, we proposed organic thin film sensor array fabricated on a curved plastic film which has finite Gauss curvature[19]. As one of the test cases, we fabricated a fingertip-shaped organic thin-film transistor (OTFT) array in this study. Possible shape of the curved surface device is not only the fingertip shape. Application of our method on various curved surfaces will be expected. We can flexibly make other curved surfaces by making proper molds. This time we tried to detect slight deformation on the fingertip shape induced by a soft touch to an object. Because organic thin film and thin plastic substrate film are sufficiently soft and flexible, we successfully detected a slight deformation which reflected induced strain distribution. Especially in this paper, we achieved not only single pixel monitoring but also real-time sequential acquisition of strain distribution by scanning 88 OTFT pixels, that was a prototype of artificial tactile sense, and numerical finite element calculation based on more realistic shape model compared to our previous work[19].

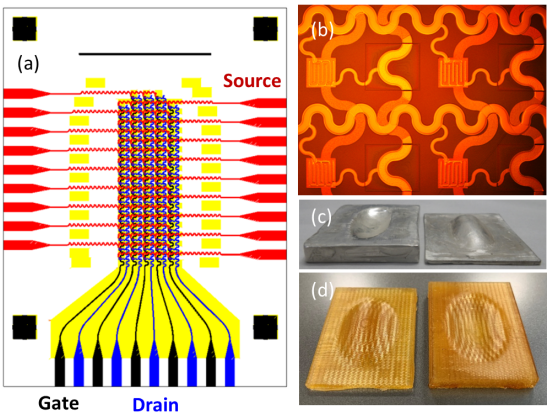

Figure 1 (a) Electrode pattern of the fingertip-shaped OTFT array. (b) Optical micrograph of OTFT array region. The electrode pattern has a redundancy to secure the tensile strain durability generated during the thermal molding. (c) Metal mold and (d) engineering plastic mold produced with 3D printer.

2 Experimental details The substrate film of thin poly(ethlene naphthalate) (PEN) that was provided from Teijin Ltd., Japan whose thickness of 75 μm was used.

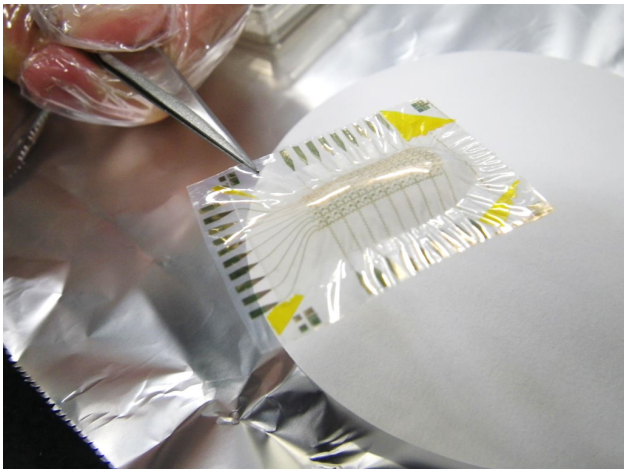

Figure 2 Photograph of the fingertip-shaped organic sensor array. Dense organic device matrix is seen in the center of the curved surface. This fingertip includes 88 organic thin film transistor as strain sensors.

Au gate electrode pattern was thermally evaporated, and 900 nm thick parylene-SR layer was formed on the substrate surface as a gate dielectric layer. Then Au contact electrode pattern was deposited on the surface, which was chemically treated by pentafluorobenzenethiol self-assembled monolayer (PFBT-SAM) to reduce the contact resistance[20–24]. Figure 1(a) shows the electrode pattern of the fingertip shaped OTFT array, and optical micrograph of OTFT array region is shown in Figure 1(b). The electrode pattern in the OTFT array region has a redundancy to secure the tensile strain durability[25,26] generated during the formation of the curved surface. A proper amount of dioctylbenzothienobenzothiophene (C_8-BTBT)[27–40] powder whose melting point was 126° C was transferred onto the substrate, and then another PEN film was put on it. Details of the sample preparation procedure are the same with our previous works[19,41,42]. In the last stage of sample preparation, the planer PEN film was deformed by thermal molding[19]. Thermal molding was carried out by clamping and pressing the planar plastic sheet with properly produced mold during thermal treatment. Figure 1 (c) and (d) show the metal and engineering plastic mold, respectively. Especially the engineering plastic mold has sufficient thermal durability, and is digitally designed and fabricated using 3D CAD and 3D printer. Figure 2 is a photograph of the fingertip-shaped device array. This sensor array includes 88 OTFTs in the center of the fingertip shaped curved surface.

This curved surface is also well fitted and stuck on the original human finger from which we made the finger mold[19]. And also, we made original tactile sense tester [19] using micro caliper to demonstrate sensitive artificial tactile sense in this work. Figure 3 (a) shows the photograph of fingertip-shaped sensor array under tactile sense test. Tip of the micro caliper head presses the top of the fingertip-shaped PEN film surface. Embedded 88 OTFT-type strain sensor array was connected to external circuit, and the readout of each pixel is carried out by the bias switching of gate voltage and drain voltage by high speed electronic relay. Figure 3 (b) shows one of the output characteristics of OTFT array fabricated in the curved surface. I_D indicates typical p-type OTFT characteristics, and I_G which include gate leakage current is sufficiently low even after the formation of the curved surface. When normal displacement to the stage plane (Δh) was applied to the top surface of the fingertip shaped sensor array, induced strain was distributed to the whole region of the curved surface, so, the strain distribution was a kind of fingerprint of the contacted objects. The contact strength and the contact point shape were reflected to the induced strain distribution collected from all sensors. We expect this electronic artificial tactile sense will easily be connected with the modern

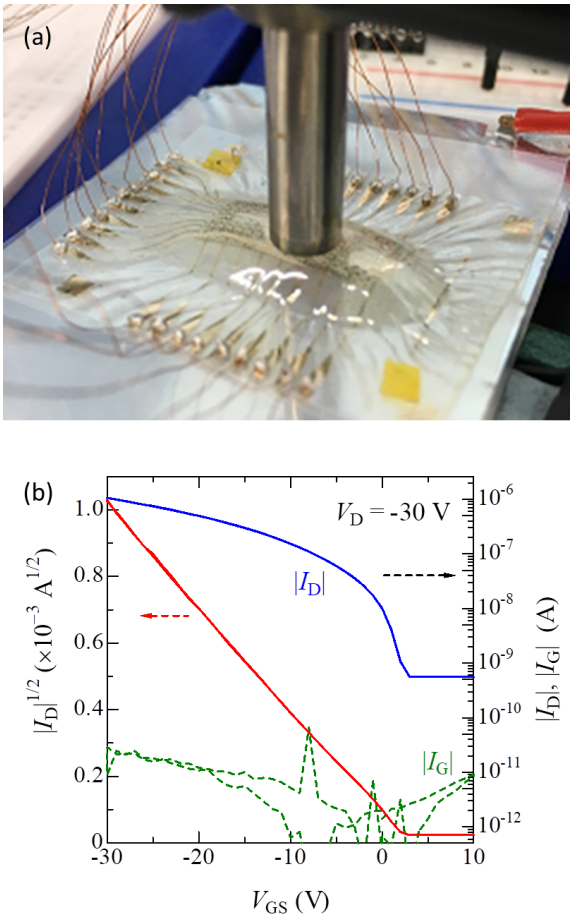

Figure 3 (a) Organic sensor array under tactile sensing test. The metal rod pressing the fingertip-shaped sensor array is the micro caliper head. Normal displacement applied to the curved surface sensor array is varied in the 100 μm resolution. (b) Typical output characteristics of the OTFT fabricated in the curved surface.

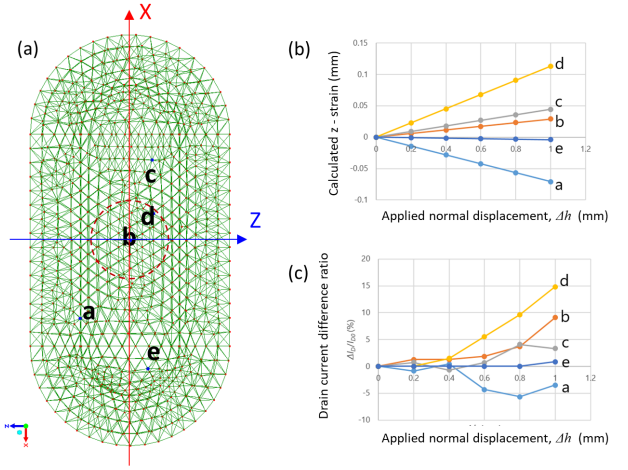

Figure 4 (a) Mesh model of the fingertip shape in the finite element method (FEM) calculation. Red circle is contact region of the micro caliper head. The points labeled from a to e are the location that FEM results were picked up. (b) Relation of the calculated strain and applied normal displacement of Δh. Differential drain current ratio of the OTFT-type strain sensors.

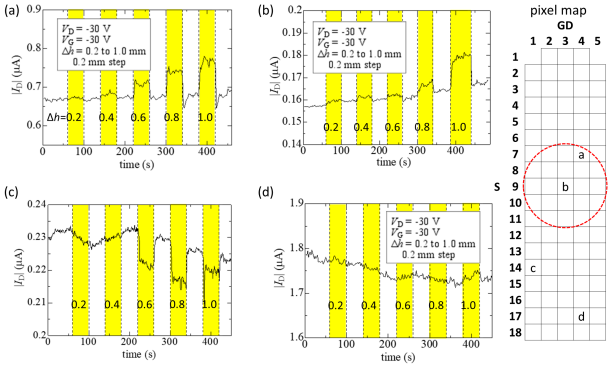

Figure 5 Time variation of the observed drain current flowing through an addressed OTFT strain sensor during the artificial tactile sensing test. Δh (0.2 - 1.0 mm) in the figure indicates applied vertical displacement from the micro caliper head.

artificial intelligence (AI) technologies, and sensitive robot finger in the precision work field will be realized in the near future.

3 Results and Discussion We carried out numerical calculations of the induced strain in the fingertip-shaped PEN film surface by the finite element method (FEM). Mesh model of the fingertip-shape shown in Figure 4 (a) was constructed and imported into the FEM simulator, LISA [43]. Characteristic points from 'a' to 'e' are marked as shown in Figure 4 (a), and the contact region is drawn as dotted brown circle. Figure 4 (b) shows the summary of the z-component of calculated induced strain at each point from 'a' to 'e' toward applied normal displacement of Δh. The reason why we picked up the z-component is that the corresponding channel direction of OTFT array is z-direction in Figure 4. This calculated results show that a compressive strain was induced in 'b', 'c', and 'd'. And the largest compressive strain was induced in point 'd' because this point belongs to the edge of the contact rod. On the other hand, tensile strain was induced in 'a', and only slight tensile strain was induced in 'e'. A strong tensile strain was induced at around 'a' because this point was located in the outer rim of the compressive strain region. Tensile strain was observed in the outer rim of the compressive strain region also in our previous simulated result in the hemisphere.[19]. And point 'e' was sufficiently far from the contact region with the test rod.

Figure 4 (c) shows summarized experimental results of drain current difference ratio ($\Delta I_{\mathrm{D}}/I_{\mathrm{D0}}$) observed in each OTFTs. At first, induced tensile and compressive strain correspond to the decrease and increase of the drain current, respectively. Positive $\Delta I_{\mathrm{D}}/I_{\mathrm{D0}}$ was observed in compressive strain region, and negative $\Delta I_{\mathrm{D}}/I_{\mathrm{D0}}$ was observed in tensile strain region because the compressive stress have effects to expand the TFT channel length, grain boundaries, and lattice parameter, all of them cause increase of electrical resistance. And for the tensile stress, effects of these factors are inverted. In addition, the absolute value of $\Delta I_{\mathrm{D}}/I_{\mathrm{D0}}$ also well corresponded to the magnitude of induced strain. As we can see, the observed drain current difference well corresponds to the calculated strain distribution, therefore, we can acquire strain distribution data electrically by distributing small OTFTs on any curved surfaces.

Figure 5 (a) is time variation of the observed drain current flowing through an addressed OTFT in 7th line and 4th row (we call S7-GD4 pixel in this paper) in the pixel map. Δh (0.2 - 1.0 mm) in the figure indicates applied vertical displacement from the micro caliper rod. This data indicate that the induced strain was compressive strain, and corresponds to the amount of Δh, and in addition, real time detection of induced strain was achieved. As recognized in the results of static measurement shown in Figure 4, this result shows the real-time monitoring of drain current in addressed OTFT pixel also accurately acquired the induced strain. Figure 5 (b) also shows the acquired compressive strain induced in S9-GD3 pixel in real time. On the other hand, Figure 5 (c) shows the detected tensile strain induced in S14-GD1 pixel during application of various Δh. And only a slight difference was observed in S17-GD4 pixel because this pixel was sufficiently far from the contact region.

Finally, we tried to make a prototype of real-time artificial tactile sense of robot finger by scanning 88 OTFTs in the sensor array using 28 high speed electrical relay (18 relays in Source side and 10 relays in Gate/Drain side) , and made a strain distribution map by building sequentially acquired $\Delta I_{\mathrm{D}}/I_{\mathrm{D0}}$ data as shown in Figure 6. By

synchronously addressing 88 OTFTs, drain current of each OTFTs was read out in 200 ms, therefore, total time required to collect 88 strain data was about 20 s in our present prototyping setup. Although present strain map is actually not constructed in real-time, it is possible to reduce the sampling time spending for each OTFT, and to reduce the number of sensing points because the human tactile sense also has distribution. Therefore, we have technical margin to improve the total response within the existing technical limit of instruments and sample design. Anyway, we have succeeded in prototyping artificial tactile sense.

Differential drain current map under three Δh from 0.2 to 1.0 mm is shown in Figure 6. As discussed in Figure 4 and Figure 5, positive and negative differential drain current corresponded to the induced compressive strain and tensile strain, respectively. In Fig. 6 (a), weak compressive strains were widely detected in the fingertip shaped curved surface, on the other hand, weak tensile strains were detected in the peripheral region. In addition, relatively rather strong tensile strain was also detected in the pixel in S6-GD3 pixel. This locally induced tensile strains were probably due to the initial direct point contact between test rod bottom and curved surface. Effect of the direct point contact on the pixel which induce the local tensile strain was possibly stronger than that of the plastic deformation of whole curved surface itself. On the other hand in Fig. 6 (b), regions of stronger compressive strains were widely distributed mainly in the vicinity of the contact circle, and tensile strains existed in the peripheral region. Both compressive and tensile strains detected by OTFT array became stronger than that of Fig.6 (a), which indicates that strains induced by touching the object were accumulated in the whole curved surface. Different from the case of bending the plane or opening the cylindrical surface and remembering the Gauss curvature of both plane and cylindrical surface is zero, strain induced in curved surface of which Gauss curvature is non-zero was accumulated by propagating generated strain in entire curved surface. And finally,

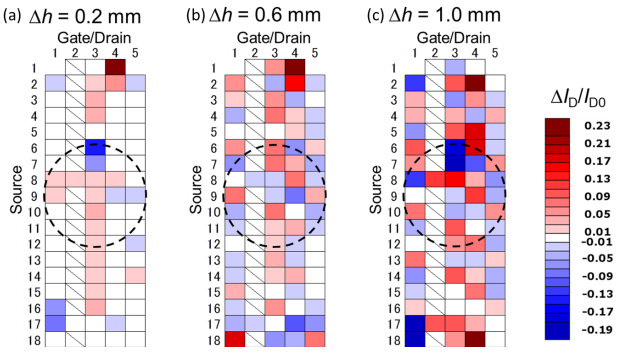

Figure 6 Differential drain current maps obtained with our real-time artificial tactile sense prototype under (a) slight touch of Δh = 0.2 mm , (b) moderate and (c) weak oppression of Δh = 1.0 mm.

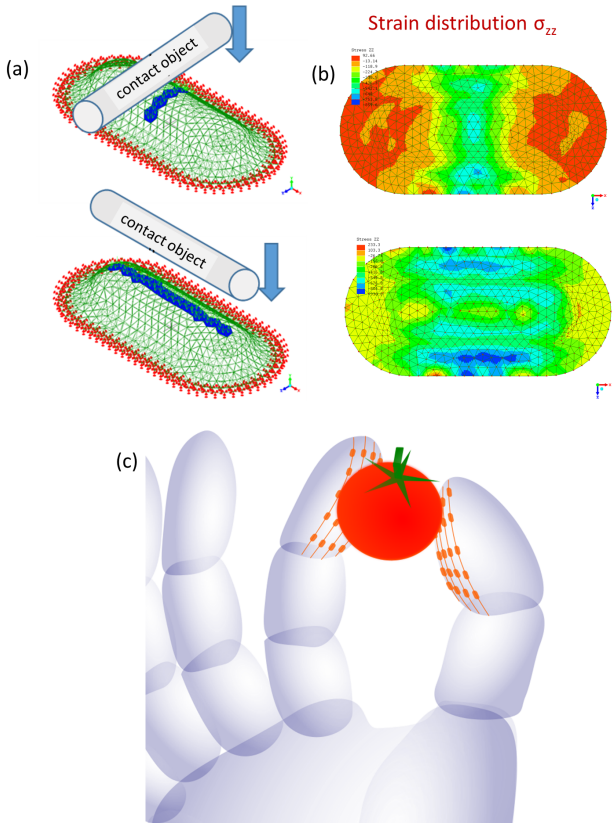

Figure 7 (a) Illustration of a bar type contact object touching the robot finger in a cross direction or a parallel direction. (b) Calculated strain distribution of σ_{zz} induced when touching a bar in a cross direction (upper) and in a parallel direction (lower) . (c) Illustration of robot finger picking up a soft and small object with properly controlled grip strength.

Fig. 6 (c) was a more deformed case. Stronger compressive strains were detected in and around the contact circle, and the observed tensile strains also increased entirely. In this way, these strain distributions, i.e. strain data at each pixel, were electrically collected in real time scale.

If the strain distributions induced by deformation of curved surface device array are electrically and dynamically collected, wide range of application can be expected. For example in this work, robot finger that has sensitive tactile sense for high precision hand works, such as repair, palpation and surgery are our passible targets. As illustrated in Fig.7 (a), if a contact object is touched to the robot finger in a cross direction and a parallel direction, induced strain distributions are different for each case as shown in Fig. 7 (b), which is calculated strain distribution of σ_{zz}. The electrically collected strain distributions are very useful to discriminate shapes and directions of objects. In addition, induced strain distribution is necessary for adjusting the grip strength to pick up soft things without crushing them as illustrated in Fig. 7 (c). Considering the speed of the recent image recognition using deep learning tech-

nologies, it is not difficult to process only 88 pixel strain data. Therefore, time delay due to the object recognition is expected to be negligible. Moreover, image recognition is also advantageous to buffer the ununiformity of sensitivity between pixels because image recognition is pattern recognition which means the acquired signal distribution is not necessarily accord with real strain distribution, in other words, absolute value of strain in each pixel is not necessary to recognize an object.

4 Summary We fabricated 88 OTFT array on a plastic film substrate and made the curved surface sensor array by thermal molding of planer device on thin plastic film. Though the demonstration of strain distribution detection in static and dynamical condition, soft robot finger that have precise tactile sense was proposed.

Acknowledgements The authors acknowledge Jun-rou Hayashi, Yushi Sasaki, Kento Watanabe, and Yuichi Miyai for their experimental help. The authors would also like to thank Teijin Ltd., Japan for providing the PEN films. This work was financially supported by a research grant from the CASIO Science Promotion Foundation. Part of this work was financially supported by JSPS fund 17H02761.

References

[1] Q. Shi, T.He, C. Lee, Nano Energy **57**, 851 (2019).
[2] M. Sugiyama, T. Uemura, M. Kondo, M. Akiyama, N. Namba, S. Yoshimoto, Y. Noda, T. Araki, and T. Sekitani , Nature Electronics, **2**, 351 (2019).
[3] T. Someya, and M. Amagai Nature Biotechnology **37** , 382 (2019).
[4] T. Araki, F. Yoshida, T. Uemura, Y. Noda, S. Yoshimoto, T. Kaiju, T. Suzuki, H. Hamanaka, K. Baba, H. Hayakawa, T. Yabumoto, H. Mochizuki, S. Kobayashi, M. Tanaka, M. Hirata, and T. Sekitani, Advanced Healthcare Materials, 1900130, (2019).
[5] R. Nur, N. Matsuhisa, Z. Jiang, M. O. G. Nayeem, T. Yokota, T. Someya, Nano Lett. **18**, 5617 (2018).
[6] T. Sekitani, S. Yoshimoto, T. Araki, and T. Uemura, SID Symposium Digest of Technical Papers, **48**, 143 (2017).
[7] X. Wang, Y. Zhang, X. Zhang, Z. Huo, X. Li, M. Que, Z. Peng, H. Wang, and C. Pan, Adv. Mater. **30**, 1706738 (2018).
[8] T. Yang, D. Xie, Z. Li, H. Zhu, Materials Science and Engineering R **115**, 1 (2017).
[9] A. Chortos, Jia Liu, and Z. Bao, Nature Mat. **15**, 937 (2016).
[10] X. Wang, H. Zhang, L. Dong, X. Han , W. Du, J. Zhai, C. Pan , and Z. L. Wang, Adv. Mater., **28**, 2896 (2016).
[11] G. Zhu, W. Q. Yang, T. Zhang, Q. Jing, J. Chen, Y. S. Zhou, P. Bai, and Z. L. Wang, Nano Lett. **14**, 3208 (2014).
[12] M. L. Hammock , A. Chortos , B. C.-K. Tee , J. B.-H. Tok , and Z. Bao, Adv. Mater. **25**, 5997 (2013).
[13] R. S. Dahiya, P. Mittendorfer, M. Valle, G. Cheng, and Vladimir J. Lumelsky, IEEE SENSORS JOURNAL, **13**, 4121 (2013).
[14] Y.-L. Park, B.-R. Chen, and R. J. Wood, IEEE SENSORS JOURNAL, **12**, 2711 (2012).
[15] M. I. Tiwana, S. J. Redmond, N. H. Lovell, Sensors and Actuators A **179** 17 (2012).
[16] H. Yousef, M. Boukallel, K. Althoefer, Sensors and Actuators A **167** 171 (2011).
[17] S. C. B. Mannsfeld, B. C-K. Tee, R. M. Stoltenberg, C. V. H-H. Chen, S. Barman, B. V. O. Muir, A. N. Sokolov, C. Reese and Z. Bao, Nature Mater. **9**, 859 (2010).
[18] H. C. Ko, M. P. Stoykovich, J. Song, V. Malyarchuk, W. M. Choi, C.-J. Yu, J. B. Geddes III, J. Xiao, S. Wang, Y. Huang and J. A. Rogers, Nature **454**, 748 (2008).
[19] M. Sakai, K. Watanabe, H. Ishimine, Y. Okada, H. Yamauchi, Y. Sadamitsu and K. Kudo, Nanoscale Research Letters **12**, 349 (2017).
[20] M. Kitamura and Y. Arakawa, Jpn. J. Appl. Phys. **50**, 01BC01 (2011).
[21] M. Kitamura, Y. Kuzumoto, S. Aomori, and Y. Arakawa, Appl. Phys. Express **4** 051601 (2011).
[22] M. Kitamura, Y. Kuzumoto, W. Kang, S. Aomori, and Y. Arakawa, Appl. Phys. Lett. **97**, 033306 (2010).
[23] Y. Kuzumoto and M Kitamura, Applied Physics Express **7**, 035701 (2014).
[24] M. Kitamura, Y. Kuzumoto, and Y. Arakawa, Physica Status Solidi (c) **10**, 1632-1635 (2013).
[25] D.S. Gray, J. Tien, C.S. Chen, Adv. Mater. **16**, 393 (2004).
[26] Y.-Y. Hsu, M. Gonzalez, F. Bossuyt, J. Vanfleteren, and I. De Wolf, IEEE Trans. Electron Devices 58, 2680 (2011).
[27] H. Ebata, T. Izawa, E. Miyazaki, K. Takimiya, M. Ikeda, H. Kuwabara, and T. Yui, J. Am. Chem. Soc. **129**, 15732 (2007).
[28] T. Uemura, Y. Hirose, M. Uno, K. Takimiya, and J. Takeya, Appl. Phys. Express **2**, 111501 (2009).
[29] T. Endo, T. Nagase, T. Kobayashi, K. Takimiya, M. Ikeda, and H. Naito, Appl. Phys. Express **3**, 121601 (2010).
[30] M. Kano, T. Minari, and K. Tsukagoshi, Appl. Phys. Express **3**, 051601 (2010).
[31] K. Takimiya, S. Shinamura, I. Osaka, and E. Miyazaki, Adv. Mater. **23**, 4347 (2011).
[32] C. Liu, T. Minari, X. Lu, A. Kumatani, K. Takimiya, and K. Tsukagoshi, Adv. Mater. **23**, 523 (2011).
[33] H. Minemawari, T. Yamada, H. Matsui, J. Tsutsumi, S. Haas, R. Chiba, R. Kumai, and T. Hasegawa, Nature **475**, 364 (2011).
[34] J. Soeda, Y. Hirose, M. Yamagishi, A. Nakao, T. Uemura, K. Nakayama, M. Uno, Y. Nakazawa, K. Takimiya, and J. Takeya, Adv. Mater. **23**, 3309 (2011).
[35] H. Tanaka, M. Kozuka, S. I. Watanabe, H. Ito, Y. Shimoi, K. Takimiya, and S. I. Kuroda, Phys. Rev. B **84**, 081306(R) (2011).
[36] T. Minari, C. Liu, M. Kano, and K. Tsukagoshi, Adv. Mater. **24**, 299 (2012).
[37] T. Minari, P. Darmawan, C. Liu, Y. Li, Y. Xu, and K. Tsukagoshi, Appl. Phys. Lett. **100**, 093303 (2012).
[38] A. Kumatani, C. Liu, Y. Li, P. Darmawan, K. Takimiya, T. Minari, and K. Tsukagoshi, Sci. Rep. **2**, 393 (2012).
[39] Y. Li, C. Liu, Y. Xu, T. Minari, P. Darmawan, and K. Tsukagoshi, Org. Electron. **13**, 815 (2012).
[40] Y. Li, C. Liu, A. Kumatani, P. Darmawan, T. Minari, and K. Tsukagoshi, Org. Electron.**13**, 264 (2012).
[41] T. Sasaki, M. Sakai, T. Ko , Y. Okada , H. Yamauchi , K. Kudo , Y. Sadamitsu , and S. Shinamura, Adv. Electron. Mater. 2, 1500221 (2016).

[42] M. Sakai, T. Koh, K. Toyoshima, K. Nakamori,Y. Okada, H. Yamauchi, Y. Sadamitsu, S. Shinamura, and K. Kudo, Phy. Rev. Applied **8**, 014001 (2017).
[43] See http://lisafea.com/ for more information about the software used for finite element simulations.

Graphical Table of Contents

GTOC image:

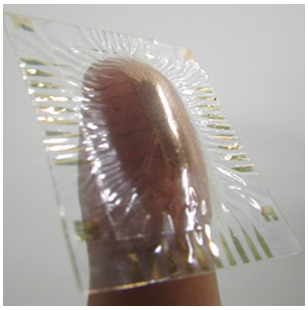

A prototype of an artificial tactile sense of a soft robot finger which is expected to substitute sensitive human finger and to be engaged in high precision works was proposed. Curved surface consist of thermally molded plastic film is effective because it has smooth shape that is faithful to the original 3D designed mold and has spring characteristics appropriate to pick up soft objects with properly controlled grip strength.